Journal of Physics:
Conference Series

PAPER • **OPEN ACCESS**

Gamma ray shielding ability of Y^{3+} doped borophosphate glasses

To cite this article: M. S. Hafiz *et al* 2024 *J. Phys.: Conf. Ser.* **2830** 012024

Journal of Physics: Conference Series **2830** (2024) 012024 doi:10.1088/1742-6596/2830/1/012024

Gamma ray shielding ability of Y^{3+} doped borophosphate glasses

M. S. Hafiz[1], M. G. El-Feky [1], Eman Ibrahim[1], N. S. Gomaa [2] and Atef El-Taher[3]

[1] Geochemical Exploration Department, Nuclear Materials Authority, P.O. Box 530, El Maadi, Cairo, Egypt.

[2] Physics Department, Faculty of Science Al-Azhar University, Nasr City ,11884, Cairo, Egypt.

[3] Physics Department, Al-Azhar University, Faculty of Science, Assuit 71452, Egypt.

maisaeed366@gmail.com

Abstract. Four selected Y_2O_3 doped borophosphate glass samples are prepared using melt quench technique. The structural properties such as density and molar volume are measured. The density (ρ) increases from 3.1384 to 3.4613 g/cm^3 whereas molar volume (V_m) decreases from 60.84 to 55.00 cm^3 mol^{-1} with addition of Y_2O_3 cm^3 mol^{-1} content. The lattice of the glasses has been tested via X-ray diffraction which is a good technique for confirming the structural properties of these glasses and FTIR spectra. In addition, radiation shielding parameters for glasses were performed theoretically utilizing XCOM program for various gamma ray energy and experimentally using NaI(Ti) scintillation detector, The glasses were irradiated using energies 0.664, 1.174 and 1.334 MeV emitted by Cs-137 and Co-60 radioactive point sources respectively. Shielding parameters as leaner (μ), mass attenuation coefficients (μ/ρ) and half value layer (HVL), tenth value layer (TVL) and mean free path (MFP). The concentration of Y_2O_3 increases the (μ/ρ) increases, the HVL, TVL, and MFP values have inverse way. Superior radiation shielding is confirmed by the glass sample containing (3%, mole) of yttrium oxide. The results show that the borophosphate glasses doped with Y_2O_3 can be used to shield gamma rays.

Keywords: Borophosphate glass; Radiation Safety; NaI (TL) scintillation detector; XCOM.

1. Introduction

The harmful gamma rays radiated from sources like nuclear in medical application must be properly controlled and shielded. These powerful and penetrating radiations can harm flora and human health. Prolonged exposure can lead to serious diseases like cancer, tissue damage, and brain failure. The damage is permanent and can be inherited. Concrete and lead-based alloys are commonly used materials for radiation protection, despite real limitations such as weight, toxicity, and opacity [1-4]. Scientists are working on creating various shielding materials such as steel [5], rocks [6], ferrites [7], alloys [8-12], and glasses [13-18]. Recent studies have focused on eco-friendly glass materials with rare earth elements for radiation detection and shielding. Glasses are amorphous materials used in radiation shielding, industry, medicine, and optics [1, 19]. Glasses are recognized for their transparency, recyclability, mechanical

strength, chemical inertness, and ability to be easily shaped and sized. Yttrium doped glass has a wide range of uses in sensor devices. Rare earth elements typically exist in a trivalent state, offering crucial thermal properties to materials. Many of these elements possess f-subshell valence electrons, as noted by Kaur et al., 2019 [20], who observed enhanced radiation shielding and sensing capabilities in lead alumino phosphate glasses doped with Sm^{3+}, Eu^{3+}, and Nd^{3+} rare-earth ions. From results we confirm that this glass is suitable for blocking gamma rays. In this study, our goal is to explore the shielding of radiation capabilities of Y^{3+} doped borophosphate glasses and study the effect of increasing Y_2O_3 concentration over wide range of gamma-ray energies.

2. Methods

2.1. Glass synthesis and methodology

We prepared four glasses were doped with rare earth elements using melt and quenching technique. The composition consisted of (62-X) % $NH_4H_2PO_4$ - 20 % B_2O_3 - 5 % ZnO - 10 % Bi_2O_3 - 3 % Na_2CO_3 - X % Y_2O_3, labeled as Y0, Y1, Y2, Y3 based on RE content with X = 0, 1, 2, 3 mol.%. High purity chemical reagents (>99.9%) were utilized, including natural Yttrium extracted using cation exchange resin Dowex 50 W-X8 of 150 mesh size from REE-concentrate sourced from Abu Zeinema gibbsite ore material. Two columns were utilized for this purpose, with the first column containing resin in its hydrogen form for preparation of the saturated REE bed, while the second column had resin in its Cu II form with a double volume. A 0.015M EDTA solution (in NH4+ form at pH 8.5) was employed as the eluant for REE from the first column to the second column at a flow rate of 1 ml/min (equivalent to a contact time of 20 min). The eluate fractions of individually separated REE were collected successfully for their pure metal values of Nd based on the stability constant difference with EDTA [19, 20]. The chemical reagents were mixed in a pestle and mortar for over 30 minutes. Samples were weighed using an electronic balance with a least count of 0.1gm. The powdered material was placed into a 40ml porcelain crucible and heated in a muffle furnace at 1100 ºC. The molten mixture was stirred continuously to prevent bubble formation. The melt was then poured into a preheated stainless-steel mold and annealed at 360 ºC for 1 hour to relieve thermal stress. Glass samples were polished to achieve maximum flatness with varying thicknesses, ranging from 0.6 to 2cm and a circular shape with a 2 cm in diameter.

2.2. Characterization of synthesized glasses

2.2.1. The Density and the Molar Volume characterization: The effect of doping Y_2O_3 on borophosphate glass was described by density and molar volume. The density of the glasses is measured using Archimedean method using toluene. The density results are about $\pm 0.001 g/cm^3$.

2.2.2. The X-ray diffraction analysis: XRD diffraction analysis is conducted at ambient temperature on glasses to be sure that the structure of the glasses is an amorphous quality using a Philips PW 3710/31 diffractometer. Before use, the device was calibrated with quartz and corundum calibration standards. It operated at 40 kV and 20 mA, using Cu Kα radiation ($\lambda = 1.54Å$) and a scan rate of 0.02 °/s. The powder was loaded onto a quartz plate and scanned from 2θ ranging from 4° to 80°.

2.2.3. The Fourier transform infrared: The glasses were studied by a Thermo scientific nicolet10 FTIR spectrophotometer over the wave number range of 2000–520 cm^{-1} at room temperature (Thermo Fisher scientific, USA).

2.2.4. WinXCom program: The current glass system's mass attenuation coefficient results were theoretically calculated with the Win-XCom software, providing partial cross-sections and total attenuation data for different elements in a large photon energy range [22].

2.2.5. The Narrow Beam Transmission Technique: The narrow beam transmission technique involves a 3"x3" NaI(Tl) scintillation detector with a 0.6 cm copper protection layer, lead brick chamber for environmental radiation isolation, 5 cm lead cover, Tennelec high voltage power supply, nuclear Enterprises shaping amplifier, and Nuclease PCA-8000 computer with 8192 multichannel analyzers. Cylindrical pellet samples are placed in a lead collimator above the detector, ensuring only a collimated beam passes through the sample layer. This technique is used for gamma rays' parameter calculation as shown in figure 1, measuring intensity Io and I photon with and without the sample pellet in place for 30 minutes [22].

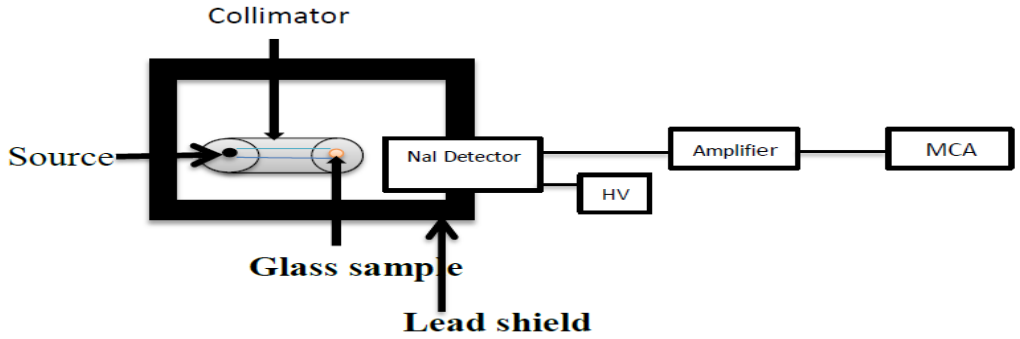

Figure1. Geometry of narrow beam transmission technique

3. Results and Discussion

3.1. The Density and the Molar Volume Measurements

The density and molar volume values of the glass samples measured show in table 1. The glass densities varied, with Y0 at 3.13 gcm^{-3} and Y3 at 3.46gcm^{-3}. The structure of the glass influences its density, as Y_2O_3 has a higher molecular mass (225.81 g/mol) than P_2O_5 (115.03 g/mol) when replacing it in the glass structure, leading to a potential increase in overall density. The molar volume decreased with more Y_2O_3 in the structure, affecting the observed variations in glass density.

Table 1. The chemical composition, density (ρ), and molar volume (V_m) of the prepared glasses.

glass Code	Composition (mol%)						Density (g/cm^3)	Molar volume ($cm^3\ mol^{-1}$)
	P_2O_5	B_2O_3	ZnO	Bi_2O_3	Na_2CO_3	Y_2O_3		
Y0	62	20	5	10	3	0	٣,١٣٨٤±0.001	٦٠,٨٤
Y1	61	20	5	10	3	1	3.4569±0.003	٥٥,٨٩
Y2	60	20	5	10	3	2	٣,٤٥٩١±0.002	٥٥,٥٠
Y3	59	20	5	10	3	3	٣,٤٦١٣±0.005	٥٥,٠٠

The arrangement of ions in the composition is better explained by molar volume (V_m) rather than density. There is an inverse relation between density and calculated molar volume of the glasses, if the density increases, molar volume decrease. The decrease in molar volume may suggest fewer void spaces causing larger density.

3.2. XRD Characteristics

The XRD configuration for the samples is validated in figure 2, XRD pattern of (Y^{3+}) in angular range $10° \leq \theta \leq 90°$.Rare of sharp peaks and broad hump at 23°-30° indicate amorphous nature instead of crystalline. This broad hump suggests amorphous nature in glass samples and halos indicate specific analysis of these glasses.

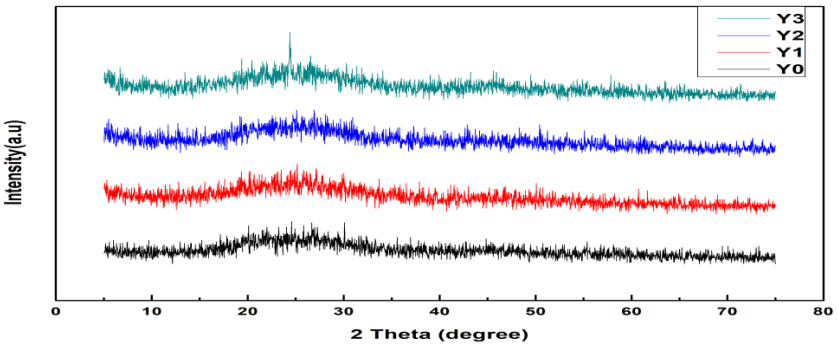

Figure 2.X-ray diffraction for glasses.

3.3. FTIR analysis

The Fourier transform infrared (FT-IR) is critical analysis which delivers a broad analysis and information about the construction of a particular structure. FT-IR presumes a vibrational-independent of the structural unit's vibrations for the glass network on the other neighbors. The FTIR peak at approximately 687 cm^{-1} corresponds to B-O vibrations connections in the borate framework as shown in figure 3.

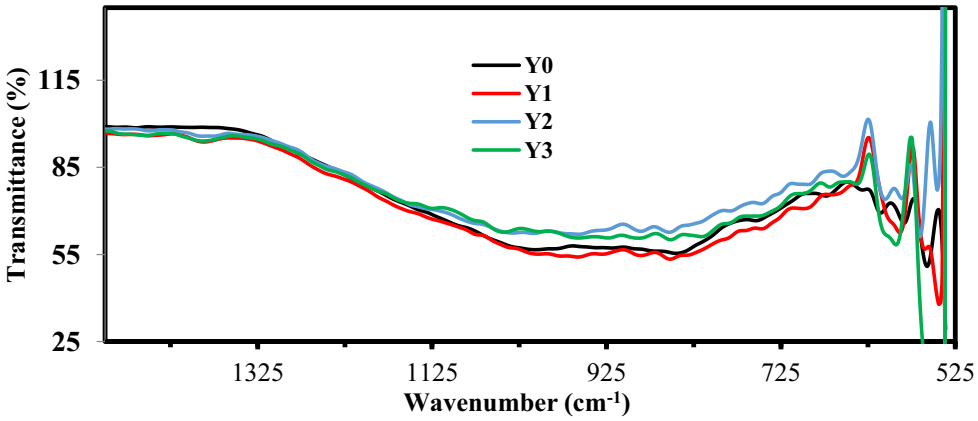

Figure 3. FTIR spectra of the glasses

A low shift to lower wavenumbers is observed with higher Y_2O_3 content, possibly due to weakened B-O bond strength from the formation of $[ZnO_{4/2}]^{2-}$ building block. Increased Y^{3+} ionic bond formation with $[BO_{4/2}]^{1-}$ could also contribute to the reduction in B-O bond strength and the shift in IR peak position. The FTIR bands in the area 800-1200 cm^{-1} are attributed to the stretching vibrations of tetrahedral BO_4 and triangular BO_3 units, respectively. Y^{3+} can coordinate with six or eight oxygen atoms, while Zn^{2+} only coordinates with four or six. This makes it easier for some Zn to be incorporated into the glass network in the form of $[ZnO_{4/2}]^{2-}$ for anionic charge compensation. Y^{3+} receives anionic compensation from borate species and to a lesser extent from zincate units. Orthoborate units are excluded due to their electrical neutrality, while $[BO_3]^{3-}$ units are excluded for generating too many negatively charged species. A six-coordinated Y^{3+} ion is bonded ionically to one $[BO_{4/2}]^{1-}$ and one $[ZnO_{4/2}]^{2-}$ unit, with B influencing the

charges of O atoms more strongly than Zn due to its lower coordination number and shorter B-O bond length. The higher radius of Y^{3+} ions may have an influence on O ions to get in contact with B ions. Therefore, the primary method of charge compensation involves interacting with $[BO_{4/2}]^{1-}$ units. Consequently, a significant number of Y^{3+} ions come into close contact with B ions to create more $[BO_{4/2}]^{1-}$ units or YBO_3 crystals with three $[BO_{4/2}]^{1-}$ units. The formation of these units is sped up as the Y_2O_3 content increases to counterbalance the rise in positive ionic modifiers. The band shows at 1024-1060 cm^{-1} is attributed to $P\text{-}O^-$ group (NBO) vibrations, from these beaks we know all changes happened in structure.

3.4. Radiation Shielding Parameters Measurements

3.4.1 The linear attenuation coefficient: The prepared glass's shielding parameters were studied using the narrow beam transmission technique, which utilized gamma energies emitted from Cs-137 and Co-60 as point sources. It was measured according to the Beer-Lambert law;

$$\mu = \frac{\mathrm{Ln}(\frac{\mathrm{Io}}{\mathrm{I}})}{\mathrm{x}} \qquad (1)$$

The intensity of the gamma photons go in and go out (Io and I) was detected experimentally by using NaI (Tl) detector [23]. The thickness (x) of the fabricated glasses was determined precisely using a micrometer with an uncertainty of ± 0.01 mm. The measured μ are shown in table 2.

Table 2. The linear attenuation coefficients of the glasses at the selected energies.

glass code	Linear attenuation coefficients μ (cm^{-1})		
	0.662 MeV	1.173 MeV	1.332 MeV
Y0	0.25± 0.01	0.18± 0.02	0.17± 0.01
Y1	0.27± 0.02	0.19± 0.04	0.18± 0.05
Y2	0.29± 0.04	0.21± 0.05	0.19± 0.03
Y3	0.31± 0.01	0.23± 0.01	0.21± 0.01

The linear increase observed in Compton scattering (CS) interaction is the primary interaction at specific energy lines of 0.662, 1.173, and 1.332 MeV, with the CS cross-section being directly proportional to atomic number Z (σ_{CS} α Z) [23]. Substituting P_2O_5 with Y_2O_3 resulted in μ values increasing from 0.25 to 0.29 cm-1 at 0.662 MeV, while increasing the Y_2O_3 ratio from 0 to 3 mol % raised μ values from 0.17 to 0.21 cm-1 at 1.332 MeV, respectively. These changes are attributed to the lower density and molecular weight of P2O5 (115.03 g/mol) being replaced by Y_2O_3 with higher density and molecular weight (225.8099 g/mol). μ values decreased as gamma-photon-energy increased due to the CS cross-section being proportional to gamma-photon-energy (σ_{CS} α E^{-1}). In this study, μ values decreased from 0.25 to 0.17 MeV for glass sample Y0 and from 0.29 to 0.20 MeV for Y3 when increasing gamma photon energy between 0.662 and 1.332 MeV.

3.4.2. The Mass attenuation coefficient (μ_m): The mass attenuation coefficient (μ_m) describes how the shielding materials attenuate the incident photons per unit density of the material. It determined experimentally by the equation [14, 15];

$$\mu_m = \mathrm{Ln}\,(\frac{\mathrm{I_o}}{\mathrm{I}})/\rho x \qquad (2)$$

In figure 4, the relationship between μ_m and yttrium oxide percentage in the glass system is presented [17, 18]. The μ_m increases as the yttrium oxide content increases for all energies but decrease with increasing energy. The behavior of the mass attenuation coefficient is similar to the linear attenuation coefficient. It rose from 0.07965 $cm^2\ g^{-1}$ for sample Y0 to 0.0837 $cm^2\ gm^{-1}$ for sample Y3 at 0.662 MeV in the glass samples of the series. The glass system's highest mass attenuation coefficient is found at 3 mol% yttrium oxide content, which consists of 59% $NH_4H_2PO_4$, 20% B_2O_3, 5 % ZnO, 10 % Bi_2O_3, 3 % Na_2CO_3, and 3 %

Y_2O_3. This glass sample has a larger concentration of doped yttrium oxide compared to other samples. Generally, an increase in the ratio of Y_2O_3 in phosphate glass systems cause an increase in (μ/ρ)

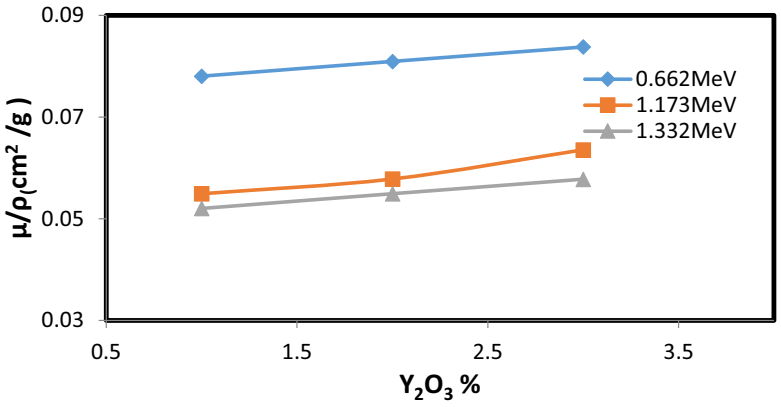

Figure 4. Mass attenuation coefficient versus Y_2O_3 content for glasses at different energies.

To confirm the correctness of the measured mass attenuation coefficients results, it is evaluated theoretically using XCOM program. A comparison of the actual and theoretical mass attenuation coefficients is presented in Table 3. The following equation may be used to calculate the percentage divergence between these two methods,

$$\text{Dev } \% = \frac{\mu_{m\,(tho)} - \mu_{m\,(exp)}}{\mu_{m\,(tho)}} \times 100. \qquad (3)$$

The deviation error between experimental and theoretical results was less than±10 %. This confirmed that there is a low difference between μ_m (ex) and μ_m (th) for the prepared phosphate doping glass with yttrium oxide at different energies. The differences between the expanded nuclear cross section libraries and the methodology databases used are what are thought to be responsible for the discrepancies between experimental and theoretical results. The glass sample Y3, with a value of 0.0837cm^2g^{-1}, has the greatest μ/ρ ratio. This number reflects 76% of the lead value when compared to the mass attenuation coefficient value of lead, which is equal to 0.1101 cm^2g^{-1}. The result confirmed the ability of phosphate glass with yttrium oxide for shielding gamma ray.

Table 3. Experimental and theoretical mass attenuation coefficients for the glasses and the corresponding deviation at different energies.

Energy	0.662		1.173		1.332	
Sample	μ_m (ex)	μ_m (th)	μ_m (ex)	μ_m (th)	μ_m (ex)	μ_m (th)
Y0	0.0795± 0.69	0.0791	0.0573 ± 1.26	0.058	0.0541 ± 0.20	0.0542
Y1	0.078± 1.32	0.079	0.0549 ± 5.41	0.058	0.052 ± 4.11	0.0543
Y2	0.081± 2.36	0.079	0.0578 ± 0.36	0.058	0.054 ± 1.31	0.0542
Y3	0.084± 9.16	0.076	0.0635 ± 9.80	0.058	0.057 ± 6.53	0.0541

3.4.3. The Half value layer, tenth value layer and Mean Free Path: The select of protecting material for use rely on Half value layer sheltering factor which definite as the thickness from protecting material that lowers the preliminary intensity of gamma rays to half its value. Tenth value layer is additional protective factor that is like HVL but it is the thickness from protecting material that decreases intensity of gamma rays to one tenth of its primary intensity according to equations.

$$\mathrm{HVL} = \frac{\ln 2}{\mu} \quad (4)$$

$$\mathrm{TVL} = \frac{\ln 10}{\mu}. \quad (5)$$

Mean free path (MFP) is the mean space between two interactions of gamma rays and protective material and can be clarified explained mathematically in relation $mfp = \frac{1}{\mu}$.Where μ is the calculated linear attenuation coefficient [23].Table 4 shows the relationship between HVL, TVL, and MFP with energy. Incorporating Y_2O_3 lowers HVL, TVL, and MFP from its high density and atomic number, increasing glass sample density. HVL decreased from 2.77, 3.85, and 4.07 cm to 2.39, 3.15, and 3.46 cm at 0.662 MeV for glass samples. TVL and MFP exhibit similar trends. A Y3 glass sample containing 59 % $NH_4H_2PO_4$, 20 % B_2O_3, 5 % ZnO, 10 % Bi_2O_3, 3 % Na_2CO_3, and 3% Y_2O_3 is the preferable sample with the lowest MFP, TVL, and HVL and highest mass attenuation coefficient due to the high Y_2O_3 content.

.

Table 4. MFP, HVL, and HVL (cm) values for glasses of prepared glass at different energies.

Sample code	0.664 MeV			1.174 MeV			1.334 MeV		
	HVL (cm)	TVL (cm)	MFP (cm)	HVL (cm)	TVL (cm)	MFP (cm)	HVL (cm)	TVL (cm)	MFP (cm)
Y0	2.75± 0.01	9.21	4.00	3.85	12.79	5.55	4.07	13.54	5.88
Y1	2.56± 0.02	8.52	3.70	3.64	12.11	5.26	3.85	12.79	5.55
Y2	2.47± 0.04	8.22	3.57	3.46	11.51	5.00	3.64	12.11	5.26
Y3	2.39± 0.01	7.93	3.44	3.15	10.46	4.54	3.46	11.51	5.00

4. Conclusion

In this work, structural and shielding characteristics of (62-X) % $NH_4H_2PO_4$-20 % B_2O_3 – 5 % ZnO -10 % Bi_2O_3-3 % Na_2CO_3 – X % Y_2O_3 by using the melt quenching technique. These glass samples are labeled as Y0, Y1, Y2, Y3 depending on RE content with x=0, 1, 2, 3mol. %, respectively glasses were investigated. A high density range from 3.13 gcm^{-3} to 3.46 gcm^{-3} characterizes the borophosphate glasses doping with varying yttrium concentration. The glass samples' amorphous nature is confirmed by the X-ray diffraction pattern, with molar volume values ranging from 60.84 cm^3 mol^{-1} to 55 cm^3 mol^{-1}. The structure of the synthesized glasses has been analyzed by FTIR spectra within the range of 525–2000 cm^{-1} at room temperature. Radiation shielding parameters for glasses were performed theoretically utilizing XCOM program for various gamma ray energy and experimentally using NaI(Ti) scintillation detector Shielding parameters. All glass samples had a high mass attenuation coefficient value along with lower HVL, TVL, and MFP values; sample Y3 had the highest mass attenuation coefficient value. There is a good agreement between the theoretical and experimental values of (μ/ρ) with deviation less than 10% between them. The best sample (Y3) has a mass attenuation coefficient value of 0.0837cm^2g^{-1}, which is 76% of lead value (0.1101 cm^2g^{-1}). The outcome shown that yttrium-doped phosphate glass effectively blocks gamma radiation.

References

[1] Al-Buriahi M. S.et al 2019 *App Phy A,* **125**.
[2] Adib M, Habib N, Bashter I, Fathallah M, Saleh A, 2011 *Ann. Nucl. Energy,* **38** pp2673–2679
[3] Singh J et al 2018 *Prog. Nucl. Energy,* **106** pp387-395.
[4] Adib M, Habib N, Bashter I, Saleh A, 2011 *Ann Nucl Energy* **38** pp 802–807.
[5] Akkurt I et al 2011 *Nucl. Eng. Des*. **241** (1) pp 55–58.
[6] Dong M et al., 2016, *J. Hazard. Mater*. **318** pp 751–757.

[7] Abdelkader O, Nasrallah M, Nasrallah M, Aleya S, Abdelkader M, Saleh A 2024 *Optical Material Express*, **14,** No. 5,1170
[8] Saleh A, Shalaby R, Abdelhakim N 2022, *Rad. Phy. Chem,* **195** 110065.
[9] Deghady A, Tayel A, Saleh A, El Basaty A 2022 *Phys. Scr.* **97** 105709
[10] Saleh A, Mansour F, Abdelhakim N 2024, *Rad. Phy. Chem,* **221** 111726.
[11] Adib M, Habib N, Bashter I, Morcos H, Fathallah M, El-Mesiry M, Saleh A 2013, *Annal. Nuc. Energy* **60** pp 163–171 Con.
[12] Saleh A, Almohiy H, Shalaby R, Saad M 2024 *Rad Phy Chem* **216** 111443.
[13] Saleh A, Elshazly R, Abd Elghany H 2021. *Arab Jour Nucl Sci Appl*, ***0*(0)** pp 1–11.
[14] Shahboub A, Saleh A, Hassan A, El Damrawi G 2023 *Appl. Phy. A,* **129**,410
[15] Saleh A 2022, Prog Nucl Energy, **154** 104482.
[16] Sayyed M, Saleh M, Kumar A, Mansour F 2024, *Nucl Eng Tech*, https://doi.org/10.1016/j.net.2024.03.038
[17] Alharbiy N, Khattari Z, Rammah Y, Saleh A 2023 *J Mater Sci: Mater Electron* **34**,191
[18] Shahboub A, El Damrawi G, Saleh A 2021 *Eur. Phys. J. Plus* **136**,947.
[19] Fawzy H , et al, 2022, **208** pp 1666-1680.
[20] Kaur P et al, 2018, *Rad Phy Chem*, **144** pp336-343.
[21] Amer T. E et al, 2009, *Isot Rad Res J* **41**(4s1) pp1163-1177.
[22] Gerward, L., et al, 2004. *Rad. Phys. Chem.,* **04**,040.
[23] Saleh A, El-Feky M, Hafiz M, Kawady N 2022 *Rad. Phys. Chem.* **202** 110586.